Study of the production of Λ_b^0 and $\overline{B}^0$ hadrons in pp collisions and first measurement of the $\Lambda_b^0 \to J/\psi p K^-$ branching fraction*

The LHCb Collaboration

R. Aaij[38], B. Adeva[37], M. Adinolfi[46], A. Affolder[52], Z. Ajaltouni[5], S. Akar[6], J. Albrecht[9], F. Alessio[38], M. Alexander[51], S. Ali[41], G. Alkhazov[30], P. Alvarez Cartelle[53], A.A. Alves Jr[57], S. Amato[2], S. Amerio[22], Y. Amhis[7], L. An[3], L. Anderlini[17], J. Anderson[40], G. Andreassi[39], M. Andreotti[16,f], J.E. Andrews[58], R.B. Appleby[54], O. Aquines Gutierrez[10], F. Archilli[38], P. d'Argent[11], A. Artamonov[35], M. Artuso[59], E. Aslanides[6], G. Auriemma[25,m], M. Baalouch[5], S. Bachmann[11], J.J. Back[48], A. Badalov[36], C. Baesso[60], W. Baldini[16,38], R.J. Barlow[54], C. Barschel[38], S. Barsuk[7], W. Barter[38], V. Batozskaya[28], V. Battista[39], A. Bay[39], L. Beaucourt[4], J. Beddow[51], F. Bedeschi[23], I. Bediaga[1], L.J. Bel[41], V. Bellee[39], N. Belloli[20,j], I. Belyaev[31], E. Ben-Haim[8], G. Bencivenni[18], S. Benson[38], J. Benton[46], A. Berezhnoy[32], R. Bernet[40], A. Bertolin[22], M.-O. Bettler[38], M. van Beuzekom[41], A. Bien[11], S. Bifani[45], P. Billoir[8], T. Bird[54], A. Birnkraut[9], A. Bizzeti[17,h], T. Blake[48], F. Blanc[39], J. Blouw[10], S. Blusk[59], V. Bocci[25], A. Bondar[34], N. Bondar[30,38], W. Bonivento[15], S. Borghi[54], M. Borsato[7], T.J.V. Bowcock[52], E. Bowen[40], C. Bozzi[16], S. Braun[11], M. Britsch[10], T. Britton[59], J. Brodzicka[54], N.H. Brook[46], E. Buchanan[46], A. Bursche[40], J. Buytaert[38], S. Cadeddu[15], R. Calabrese[16,f], M. Calvi[20,j], M. Calvo Gomez[36,o], P. Campana[18], D. Campora Perez[38], L. Capriotti[54], A. Carbone[14,d], G. Carboni[24,k], R. Cardinale[19,i], A. Cardini[15], P. Carniti[20,j], L. Carson[50], K. Carvalho Akiba[2,38], G. Casse[52], L. Cassina[20,j], L. Castillo Garcia[38], M. Cattaneo[38], Ch. Cauet[9], G. Cavallero[19], R. Cenci[23,s], M. Charles[8], Ph. Charpentier[38], M. Chefdeville[4], S. Chen[54], S.-F. Cheung[55], N. Chiapolini[40], M. Chrzaszcz[40], X. Cid Vidal[38], G. Ciezarek[41], P.E.L. Clarke[50], M. Clemencic[38], H.V. Cliff[47], J. Closier[38], V. Coco[38], J. Cogan[6], E. Cogneras[5], V. Cogoni[15,e], L. Cojocariu[29], G. Collazuol[22], P. Collins[38], A. Comerma-Montells[11], A. Contu[15,38], A. Cook[46], M. Coombes[46], S. Coquereau[8], G. Corti[38], M. Corvo[16,f], B. Couturier[38], G.A. Cowan[50], D.C. Craik[48], A. Crocombe[48], M. Cruz Torres[60], S. Cunliffe[53], R. Currie[53], C. D'Ambrosio[38], E. Dall'Occo[41], J. Dalseno[46], P.N.Y. David[41], A. Davis[57], K. De Bruyn[6], S. De Capua[54], M. De Cian[11], J.M. De Miranda[1], L. De Paula[2], P. De Simone[18], C.-T. Dean[51], D. Decamp[4], M. Deckenhoff[9], L. Del Buono[8], N. Déléage[4], M. Demmer[9], D. Derkach[65], O. Deschamps[5], F. Dettori[38], B. Dey[21], A. Di Canto[38], F. Di Ruscio[24], H. Dijkstra[38], S. Donleavy[52], F. Dordei[11], M. Dorigo[39], A. Dosil Suárez[37], D. Dossett[48], A. Dovbnya[43], K. Dreimanis[52], L. Dufour[41], G. Dujany[54], F. Dupertuis[39], P. Durante[38], R. Dzhelyadin[35], A. Dziurda[26], A. Dzyuba[30], S. Easo[49,38], U. Egede[53], V. Egorychev[31], S. Eidelman[34], S. Eisenhardt[50], U. Eitschberger[9], R. Ekelhof[9], L. Eklund[51], I. El Rifai[5], Ch. Elsasser[40], S. Ely[59], S. Esen[11], H.M. Evans[47], T. Evans[55], A. Falabella[14], C. Färber[38], N. Farley[45], S. Farry[52], R. Fay[52], D. Ferguson[50], V. Fernandez Albor[37], F. Ferrari[14], F. Ferreira Rodrigues[1], M. Ferro-Luzzi[38], S. Filippov[33], M. Fiore[16,38,f], M. Fiorini[16,f], M. Firlej[27], C. Fitzpatrick[39], T. Fiutowski[27], K. Fohl[38], P. Fol[53], M. Fontana[15], F. Fontanelli[19,i], R. Forty[38], O. Francisco[2], M. Frank[38], C. Frei[38], M. Frosini[17], J. Fu[21], E. Furfaro[24,k], A. Gallas Torreira[37], D. Galli[14,d], S. Gallorini[22,38], S. Gambetta[50], M. Gandelman[2], P. Gandini[55], Y. Gao[3], J. García Pardiñas[37], J. Garra Tico[47], L. Garrido[36], D. Gascon[36], C. Gaspar[38], R. Gauld[55], L. Gavardi[9], G. Gazzoni[5], D. Gerick[11], E. Gersabeck[11], M. Gersabeck[54], T. Gershon[48], Ph. Ghez[4], S. Gianì[39], V. Gibson[47], O. G. Girard[39], L. Giubega[29], V.V. Gligorov[38], C. Göbel[60], D. Golubkov[31], A. Golutvin[53,31,38], A. Gomes[1,a], C. Gotti[20,j], M. Grabalosa Gándara[5], R. Graciani Diaz[36], L.A. Granado Cardoso[38], E. Graugés[36], E. Graverini[40], G. Graziani[17], A. Grecu[29], E. Greening[55], S. Gregson[47], P. Griffith[45], L. Grillo[11], O. Grünberg[63], B. Gui[59], E. Gushchin[33], Yu. Guz[35,38], T. Gys[38], T. Hadavizadeh[55], C. Hadjivasiliou[59], G. Haefeli[39], C. Haen[38], S.C. Haines[47], S. Hall[53], B. Hamilton[58], X. Han[11], S. Hansmann-Menzemer[11], N. Harnew[55], S.T. Harnew[46], J. Harrison[54], J. He[38], T. Head[39], V. Heijne[41], K. Hennessy[52], P. Henrard[5], L. Henry[8], E. van Herwijnen[38], M. Heß[63], A. Hicheur[2], D. Hill[55], M. Hoballah[5], C. Hombach[54], W. Hulsbergen[41], T. Humair[53], N. Hussain[55], D. Hutchcroft[52], D. Hynds[51], M. Idzik[27], P. Ilten[56], R. Jacobsson[38], A. Jaeger[11], J. Jalocha[55], E. Jans[41], A. Jawahery[58], F. Jing[3], M. John[55], D. Johnson[38], C.R. Jones[47], C. Joram[38], B. Jost[38], N. Jurik[59], S. Kandybei[43], W. Kanso[6], M. Karacson[38], T.M. Karbach[38,†], S. Karodia[51], M. Kecke[11], M. Kelsey[59], I.R. Kenyon[45], M. Kenzie[38], T. Ketel[42], B. Khanji[20,38,j], C. Khurewathanakul[39], S. Klaver[54], K. Klimaszewski[28],

Received 1 September 2015

*Supported by CERN and national agencies: CAPES, CNPq, FAPERJ and FINEP (Brazil); NSFC (China); CNRS/IN2P3 (France); BMBF, DFG, HGF and MPG (Germany); INFN (Italy); FOM and NWO (The Netherlands); MNiSW and NCN (Poland); MEN/IFA (Romania); MinES and FANO (Russia); MinECo (Spain); SNSF and SER (Switzerland); NASU (Ukraine); STFC (United Kingdom); NSF (USA). The Tier1 computing centres are supported by IN2P3 (France), KIT and BMBF (Germany), INFN (Italy), NWO and SURF (The Netherlands), PIC (Spain), GridPP (United Kingdom). Individual groups or members have received support from EPLANET, Marie Skłodowska-Curie Actions and ERC (European Union), Conseil général de Haute-Savoie, Labex ENIGMASS and OCEVU, Région Auvergne (France), RFBR (Russia), XuntaGal and GENCAT (Spain), Royal Society and Royal Commission for the Exhibition of 1851 (United Kingdom).

O. Kochebina[7], M. Kolpin[11], I. Komarov[39], R.F. Koopman[42], P. Koppenburg[41,38], M. Kozeiha[5], L. Kravchuk[33], K. Kreplin[11], M. Kreps[48], G. Krocker[11], P. Krokovny[34], F. Kruse[9], W. Krzemien[28], W. Kucewicz[26,n], M. Kucharczyk[26], V. Kudryavtsev[34], A. K. Kuonen[39], K. Kurek[28], T. Kvaratskheliya[31], D. Lacarrere[38], G. Lafferty[54], A. Lai[15], D. Lambert[50], G. Lanfranchi[18], C. Langenbruch[48], B. Langhans[38], T. Latham[48], C. Lazzeroni[45], R. Le Gac[6], J. van Leerdam[41], J.-P. Lees[4], R. Lefèvre[5], A. Leflat[32,38], J. Lefrançois[7], E. Lemos Cid[37], O. Leroy[6], T. Lesiak[26], B. Leverington[11], Y. Li[7], T. Likhomanenko[65,64], M. Liles[52], R. Lindner[38], C. Linn[38], F. Lionetto[40], B. Liu[15], X. Liu[3], D. Loh[48], I. Longstaff[51], J.H. Lopes[2], D. Lucchesi[22,q], M. Lucio Martinez[37], H. Luo[50], A. Lupato[22], E. Luppi[16,f], O. Lupton[55], A. Lusiani[23], F. Machefert[7], F. Maciuc[29], O. Maev[30], K. Maguire[54], S. Malde[55], A. Malinin[64], G. Manca[7], G. Mancinelli[6], P. Manning[59], A. Mapelli[38], J. Maratas[5], J.F. Marchand[4], U. Marconi[14], C. Marin Benito[36], P. Marino[23,38,s], J. Marks[11], G. Martellotti[25], M. Martin[6], M. Martinelli[39], D. Martinez Santos[37], F. Martinez Vidal[66], D. Martins Tostes[2], A. Massafferri[1], R. Matev[38], A. Mathad[48], Z. Mathe[38], C. Matteuzzi[20], A. Mauri[40], B. Maurin[39], A. Mazurov[45], M. McCann[53], J. McCarthy[45], A. McNab[54], R. McNulty[12], B. Meadows[57], F. Meier[9], M. Meissner[11], D. Melnychuk[28], M. Merk[41], E Michielin[22], D.A. Milanes[62], M.-N. Minard[4], D.S. Mitzel[11], J. Molina Rodriguez[60], I.A. Monroy[62], S. Monteil[5], M. Morandin[22], P. Morawski[27], A. Mordà[6], M.J. Morello[23,s], J. Moron[27], A.B. Morris[50], R. Mountain[59], F. Muheim[50], D. Müller[54], J. Müller[9], K. Müller[40], V. Müller[9], M. Mussini[14], B. Muster[39], P. Naik[46], T. Nakada[39], R. Nandakumar[49], A. Nandi[55], I. Nasteva[2], M. Needham[50], N. Neri[21], S. Neubert[11], N. Neufeld[38], M. Neuner[11], A.D. Nguyen[39], T.D. Nguyen[39], C. Nguyen-Mau[39,p], V. Niess[5], R. Niet[9], N. Nikitin[32], T. Nikodem[11], D. Ninci[23], A. Novoselov[35], D.P. O'Hanlon[48], A. Oblakowska-Mucha[27], V. Obraztsov[35], S. Ogilvy[51], O. Okhrimenko[44], R. Oldeman[15,e], C.J.G. Onderwater[67], B. Osorio Rodrigues[1], J.M. Otalora Goicochea[2], A. Otto[38], P. Owen[53], A. Oyanguren[66], A. Palano[13,c], F. Palombo[21,t], M. Palutan[18], J. Panman[38], A. Papanestis[49], M. Pappagallo[51], L.L. Pappalardo[16,f], C. Pappenheimer[57], C. Parkes[54], G. Passaleva[17], G.D. Patel[52], M. Patel[53], C. Patrignani[19,i], A. Pearce[54,49], A. Pellegrino[41], G. Penso[25,l], M. Pepe Altarelli[38], S. Perazzini[14,d], P. Perret[5], L. Pescatore[45], K. Petridis[46], A. Petrolini[19,i], M. Petruzzo[21], E. Picatoste Olloqui[36], B. Pietrzyk[4], T. Pilař[48], D. Pinci[25], A. Pistone[19], A. Piucci[11], S. Playfer[50], M. Plo Casasus[37], T. Poikela[38], F. Polci[8], A. Poluektov[48,34], I. Polyakov[31], E. Polycarpo[2], A. Popov[35], D. Popov[10,38], B. Popovici[29], C. Potterat[2], E. Price[46], J.D. Price[52], J. Prisciandaro[39], A. Pritchard[52], C. Prouve[46], V. Pugatch[44], A. Puig Navarro[39], G. Punzi[23,r], W. Qian[4], R. Quagliani[7,46], B. Rachwal[26], J.H. Rademacker[46], M. Rama[23], M.S. Rangel[2], I. Raniuk[43], N. Rauschmayr[38], G. Raven[42], F. Redi[53], S. Reichert[54], M.M. Reid[48], A.C. dos Reis[1], S. Ricciardi[49], S. Richards[46], M. Rihl[38], K. Rinnert[52], V. Rives Molina[36], P. Robbe[7,38], A.B. Rodrigues[1], E. Rodrigues[54], J.A. Rodriguez Lopez[62], P. Rodriguez Perez[54], S. Roiser[38], V. Romanovsky[35], A. Romero Vidal[37], J. W. Ronayne[12], M. Rotondo[22], J. Rouvinet[39], T. Ruf[38], P. Ruiz Valls[66], J.J. Saborido Silva[37], N. Sagidova[30], P. Sail[51], B. Saitta[15,e], V. Salustino Guimaraes[2], C. Sanchez Mayordomo[66], B. Sanmartin Sedes[37], R. Santacesaria[25], C. Santamarina Rios[37], M. Santimaria[18], E. Santovetti[24,k], A. Sarti[18,l], C. Satriano[25,m], A. Satta[24], D.M. Saunders[46], D. Savrina[31,32], M. Schiller[38], H. Schindler[38], M. Schlupp[9], M. Schmelling[10], T. Schmelzer[9], B. Schmidt[38], O. Schneider[39], A. Schopper[38], M. Schubiger[39], M.-H. Schune[7], R. Schwemmer[38], B. Sciascia[18], A. Sciubba[25,l], A. Semennikov[31], N. Serra[40], J. Serrano[6], L. Sestini[22], P. Seyfert[20], M. Shapkin[35], I. Shapoval[16,43,f], Y. Shcheglov[30], T. Shears[52], L. Shekhtman[34], V. Shevchenko[64], A. Shires[9], B.G. Siddi[16], R. Silva Coutinho[48,40], L. Silva de Oliveira[2], G. Simi[22], M. Sirendi[47], N. Skidmore[46], T. Skwarnicki[59], E. Smith[55,49], E. Smith[53], I. T. Smith[50], J. Smith[47], M. Smith[54], H. Snoek[41], M.D. Sokoloff[57,38], F.J.P. Soler[51], F. Soomro[39], D. Souza[46], B. Souza De Paula[2], B. Spaan[9], P. Spradlin[51], S. Sridharan[38], F. Stagni[38], M. Stahl[11], S. Stahl[38], S. Stefkova[53], O. Steinkamp[40], O. Stenyakin[35], S. Stevenson[55], S. Stoica[29], S. Stone[59], B. Storaci[40], S. Stracka[23,s], M. Straticiuc[29], U. Straumann[40], L. Sun[57], W. Sutcliffe[53], K. Swientek[27], S. Swientek[9], V. Syropoulos[42], M. Szczekowski[28], P. Szczypka[39,38], T. Szumlak[27], S. T'Jampens[4], A. Tayduganov[6], T. Tekampe[9], M. Teklishyn[7], G. Tellarini[16,f], F. Teubert[38], C. Thomas[55], E. Thomas[38], J. van Tilburg[41], V. Tisserand[4], M. Tobin[39], J. Todd[57], S. Tolk[42], L. Tomassetti[16,f], D. Tonelli[38], S. Topp-Joergensen[55], N. Torr[55], E. Tournefier[4], S. Tourneur[39], K. Trabelsi[39], M.T. Tran[39], M. Tresch[40], A. Trisovic[38], A. Tsaregorodtsev[6], P. Tsopelas[41], N. Tuning[41,38], A. Ukleja[28], A. Ustyuzhanin[65,64], U. Uwer[11], C. Vacca[15,e], V. Vagnoni[14], G. Valenti[14], A. Vallier[7], R. Vazquez Gomez[18], P. Vazquez Regueiro[37], C. Vázquez Sierra[37], S. Vecchi[16], J.J. Velthuis[46], M. Veltri[17,g], G. Veneziano[39], M. Vesterinen[11], B. Viaud[7], D. Vieira[2], M. Vieites Diaz[37], X. Vilasis-Cardona[36,o], V. Volkov[32], A. Vollhardt[40], D. Volyanskyy[10], D. Voong[46], A. Vorobyev[30], V. Vorobyev[34], C. Voß[63], J.A. de Vries[41], R. Waldi[63], C. Wallace[48], R. Wallace[12], J. Walsh[23], S. Wandernoth[11], J. Wang[59], D.R. Ward[47], N.K. Watson[45], D. Websdale[53], A. Weiden[40], M. Whitehead[48], G. Wilkinson[55,38], M. Wilkinson[59], M. Williams[38], M.P. Williams[45], M. Williams[56], T. Williams[45], F.F. Wilson[49], J. Wimberley[58], J. Wishahi[9], W. Wislicki[28], M. Witek[26], G. Wormser[7], S.A. Wotton[47], S. Wright[47], K. Wyllie[38], Y. Xie[61], Z. Xu[39], Z. Yang[3], J. Yu[61], X. Yuan[34], O. Yushchenko[35], M. Zangoli[14], M. Zavertyaev[10,b], L. Zhang[3], Y. Zhang[3], A. Zhelezov[11], A. Zhokhov[31], L. Zhong[3], S. Zucchelli[14]

[1]Centro Brasileiro de Pesquisas Físicas (CBPF), Rio de Janeiro, Brazil
[2]Universidade Federal do Rio de Janeiro (UFRJ), Rio de Janeiro, Brazil
[3]Center for High Energy Physics, Tsinghua University, Beijing, China
[4]LAPP, Université Savoie Mont-Blanc, CNRS/IN2P3, Annecy-Le-Vieux, France
[5]Clermont Université, Université Blaise Pascal, CNRS/IN2P3, LPC, Clermont-Ferrand, France
[6]CPPM, Aix-Marseille Université, CNRS/IN2P3, Marseille, France
[7]LAL, Université Paris-Sud, CNRS/IN2P3, Orsay, France

[8]LPNHE, Université Pierre et Marie Curie, Université Paris Diderot, CNRS/IN2P3, Paris, France
[9]Fakultät Physik, Technische Universität Dortmund, Dortmund, Germany
[10]Max-Planck-Institut für Kernphysik (MPIK), Heidelberg, Germany
[11]Physikalisches Institut, Ruprecht-Karls-Universität Heidelberg, Heidelberg, Germany
[12]School of Physics, University College Dublin, Dublin, Ireland
[13]Sezione INFN di Bari, Bari, Italy
[14]Sezione INFN di Bologna, Bologna, Italy
[15]Sezione INFN di Cagliari, Cagliari, Italy
[16]Sezione INFN di Ferrara, Ferrara, Italy
[17]Sezione INFN di Firenze, Firenze, Italy
[18]Laboratori Nazionali dell'INFN di Frascati, Frascati, Italy
[19]Sezione INFN di Genova, Genova, Italy
[20]Sezione INFN di Milano Bicocca, Milano, Italy
[21]Sezione INFN di Milano, Milano, Italy
[22]Sezione INFN di Padova, Padova, Italy
[23]Sezione INFN di Pisa, Pisa, Italy
[24]Sezione INFN di Roma Tor Vergata, Roma, Italy
[25]Sezione INFN di Roma La Sapienza, Roma, Italy
[26]Henryk Niewodniczanski Institute of Nuclear Physics Polish Academy of Sciences, Kraków, Poland
[27]AGH - University of Science and Technology, Faculty of Physics and Applied Computer Science, Kraków, Poland
[28]National Center for Nuclear Research (NCBJ), Warsaw, Poland
[29]Horia Hulubei National Institute of Physics and Nuclear Engineering, Bucharest-Magurele, Romania
[30]Petersburg Nuclear Physics Institute (PNPI), Gatchina, Russia
[31]Institute of Theoretical and Experimental Physics (ITEP), Moscow, Russia
[32]Institute of Nuclear Physics, Moscow State University (SINP MSU), Moscow, Russia
[33]Institute for Nuclear Research of the Russian Academy of Sciences (INR RAN), Moscow, Russia
[34]Budker Institute of Nuclear Physics (SB RAS) and Novosibirsk State University, Novosibirsk, Russia
[35]Institute for High Energy Physics (IHEP), Protvino, Russia
[36]Universitat de Barcelona, Barcelona, Spain
[37]Universidad de Santiago de Compostela, Santiago de Compostela, Spain
[38]European Organization for Nuclear Research (CERN), Geneva, Switzerland
[39]Ecole Polytechnique Fédérale de Lausanne (EPFL), Lausanne, Switzerland
[40]Physik-Institut, Universität Zürich, Zürich, Switzerland
[41]Nikhef National Institute for Subatomic Physics, Amsterdam, The Netherlands
[42]Nikhef National Institute for Subatomic Physics and VU University Amsterdam, Amsterdam, The Netherlands
[43]NSC Kharkiv Institute of Physics and Technology (NSC KIPT), Kharkiv, Ukraine
[44]Institute for Nuclear Research of the National Academy of Sciences (KINR), Kyiv, Ukraine
[45]University of Birmingham, Birmingham, United Kingdom
[46]H.H. Wills Physics Laboratory, University of Bristol, Bristol, United Kingdom
[47]Cavendish Laboratory, University of Cambridge, Cambridge, United Kingdom
[48]Department of Physics, University of Warwick, Coventry, United Kingdom
[49]STFC Rutherford Appleton Laboratory, Didcot, United Kingdom
[50]School of Physics and Astronomy, University of Edinburgh, Edinburgh, United Kingdom
[51]School of Physics and Astronomy, University of Glasgow, Glasgow, United Kingdom
[52]Oliver Lodge Laboratory, University of Liverpool, Liverpool, United Kingdom
[53]Imperial College London, London, United Kingdom
[54]School of Physics and Astronomy, University of Manchester, Manchester, United Kingdom
[55]Department of Physics, University of Oxford, Oxford, United Kingdom
[56]Massachusetts Institute of Technology, Cambridge, MA, United States
[57]University of Cincinnati, Cincinnati, OH, United States
[58]University of Maryland, College Park, MD, United States
[59]Syracuse University, Syracuse, NY, United States
[60]Pontifícia Universidade Católica do Rio de Janeiro (PUC-Rio), Rio de Janeiro, Brazil, associated to [2]
[61]Institute of Particle Physics, Central China Normal University, Wuhan, Hubei, China, associated to [3]
[62]Departamento de Fisica , Universidad Nacional de Colombia, Bogota, Colombia, associated to [8]
[63]Institut für Physik, Universität Rostock, Rostock, Germany, associated to [11]
[64]National Research Centre Kurchatov Institute, Moscow, Russia, associated to [31]
[65]Yandex School of Data Analysis, Moscow, Russia, associated to [31]
[66]Instituto de Fisica Corpuscular (IFIC), Universitat de Valencia-CSIC, Valencia, Spain, associated to [36]
[67]Van Swinderen Institute, University of Groningen, Groningen, The Netherlands, associated to [41]

[a]Universidade Federal do Triângulo Mineiro (UFTM), Uberaba-MG, Brazil
[b]P.N. Lebedev Physical Institute, Russian Academy of Science (LPI RAS), Moscow, Russia
[c]Università di Bari, Bari, Italy
[d]Università di Bologna, Bologna, Italy
[e]Università di Cagliari, Cagliari, Italy
[f]Università di Ferrara, Ferrara, Italy
[g]Università di Urbino, Urbino, Italy

[h]Università di Modena e Reggio Emilia, Modena, Italy
[i]Università di Genova, Genova, Italy
[j]Università di Milano Bicocca, Milano, Italy
[k]Università di Roma Tor Vergata, Roma, Italy
[l]Università di Roma La Sapienza, Roma, Italy
[m]Università della Basilicata, Potenza, Italy
[n]AGH - University of Science and Technology, Faculty of Computer Science, Electronics and Telecommunications, Kraków, Poland
[o]LIFAELS, La Salle, Universitat Ramon Llull, Barcelona, Spain
[p]Hanoi University of Science, Hanoi, Viet Nam
[q]Università di Padova, Padova, Italy
[r]Università di Pisa, Pisa, Italy
[s]Scuola Normale Superiore, Pisa, Italy
[t]Università degli Studi di Milano, Milano, Italy

[†]Deceased

Abstract: The product of the Λ_b^0 ($\overline{B}^0$) differential production cross-section and the branching fraction of the decay $\Lambda_b^0 \to J/\psi\, pK^-$ ($\overline{B}^0 \to J/\psi \overline{K}^*(892)^0$) is measured as a function of the beauty hadron transverse momentum, p_T, and rapidity, y. The kinematic region of the measurements is $p_T < 20$ GeV/c and $2.0 < y < 4.5$. The measurements use a data sample corresponding to an integrated luminosity of $3\,fb^{-1}$ collected by the LHCb detector in pp collisions at centre-of-mass energies $\sqrt{s} = 7$ TeV in 2011 and $\sqrt{s} = 8$ TeV in 2012. Based on previous LHCb results of the fragmentation fraction ratio, $f_{\Lambda_b^0}/f_d$, the branching fraction of the decay $\Lambda_b^0 \to J/\psi\, pK^-$ is measured to be

$$\mathcal{B}(\Lambda_b^0 \to J/\psi\, pK^-) = (3.17 \pm 0.04 \pm 0.07 \pm 0.34^{+0.45}_{-0.28}) \times 10^{-4},$$

where the first uncertainty is statistical, the second is systematic, the third is due to the uncertainty on the branching fraction of the decay $\overline{B}^0 \to J/\psi \overline{K}^*(892)^0$, and the fourth is due to the knowledge of $f_{\Lambda_b^0}/f_d$. The sum of the asymmetries in the production and decay between Λ_b^0 and $\overline{\Lambda}_b^0$ is also measured as a function of p_T and y. The previously published branching fraction of $\Lambda_b^0 \to J/\psi\, p\pi^-$, relative to that of $\Lambda_b^0 \to J/\psi\, pK^-$, is updated. The branching fractions of $\Lambda_b^0 \to P_c^+(\to J/\psi\, p)K^-$ are determined.

Keywords: production cross-section, branching fraction, b hadrons, proton-proton collisions

PACS: 14.20.Mr, 13.30.Eg, 13.75.Cs **DOI:** 10.1088/1674-1137/40/1/011001

1 Introduction

In quantum chromodynamics (QCD) the production process of b hadrons can be divided into two steps, assuming factorisation: a hard process for b production and a soft process to describe hadronisation. The hard process can be predicted by perturbative calculations in QCD; the soft process is parameterised by the fragmentation function, which has large uncertainties due to non-perturbative QCD contributions. The study of the production of b hadrons tests the factorisation ansatz. The ground state of the b-baryon family, Λ_b^0, has a wide range of decay modes. The study of its production and decays can offer complementary information to that obtained from the study of B mesons. The kinematic dependence of the production of Λ_b^0 baryons relative to that of B mesons can test differences in the b quark hadronisation process between the two [1, 2]. Furthermore, the asymmetry of heavy flavoured baryons and antibaryons produced in pp collisions is an important input for various asymmetry measurements. Leading-order QCD calculations predict equal production cross-sections for heavy baryons and heavy anti-baryons, while measurements at the ISR showed that Λ_c^+ production is favoured in pp collisions at forward rapidity, y [3, 4]. The CMS experiment measured the Λ_b^0 and $\overline{\Lambda}_b^0$ production ratio in pp collisions at 7 TeV, and no asymmetry was observed, but the large uncertainties preclude definitive conclusions [5]. Measurements at LHCb can provide further tests of existing mechanisms, e.g., the string drag effect or the leading quark effect [6].

Measurements of Λ_b^0 production to date have mostly been based on semileptonic decays and the hadronic decays $\Lambda_b^0 \to J/\psi\,\Lambda$ and $\Lambda_b^0 \to \Lambda_c^+\pi^-$ (charge-conjugation is implied throughout the paper unless otherwise specified). Using semileptonic decays, the LHCb experiment measured the ratio of Λ_b^0 baryon production to light B meson production, $f_{\Lambda_b^0}/(f_u + f_d)$ [7]. The kinematic dependence of the ratio of Λ_b^0 to $\overline{B}^0$ production, $f_{\Lambda_b^0}/f_d$, was measured using $\Lambda_b^0 \to \Lambda_c^+\pi^-$ and $\overline{B}^0 \to D^+\pi^-$ decays, and the absolute branching fraction $\mathcal{B}(\Lambda_b^0 \to \Lambda_c^+\pi^-)$ was determined [8].

In this paper, the Λ_b^0 candidates are reconstructed in the decay channel $\Lambda_b^0 \to J/\psi\, pK^-$, which was first observed by LHCb in 2013 [9]. Compared with the open-charm decays of Λ_b^0 baryons, this channel has higher trig-

ger efficiencies, especially in the region of low transverse momentum, $p_{\rm T}$. Two pentaquark-charmonium states $\rm P_c(4380)^+$ and $\rm P_c(4450)^+$ were observed by LHCb [10] in the amplitude analysis of the $\Lambda_{\rm b}^0\to {\rm J/\psi\, pK^-}$ decay. The measurement of the absolute branching fraction of $\Lambda_{\rm b}^0\to {\rm J/\psi\, pK^-}$ in the current paper allows the pentaquark branching fractions to be determined. Other $\Lambda_{\rm b}^0$ decays with a charmonium meson in the final state, such as the Cabibbo-suppressed decay $\Lambda_{\rm b}^0\to {\rm J/\psi\, p\pi^-}$ [11], can use the $\Lambda_{\rm b}^0\to {\rm J/\psi\, pK^-}$ decay as a reference to measure their absolute branching fractions.

The product of the $\Lambda_{\rm b}^0$ ($\overline{\rm B}^0$) differential production cross-section and the branching fraction of the $\Lambda_{\rm b}^0\to {\rm J/\psi\, pK^-}$ ($\overline{\rm B}^0\to {\rm J/\psi}\overline{\rm K}^{*0}$) decay is measured as a function of $p_{\rm T}$ and y, where $\overline{\rm K}^{*0}$ indicates the $\overline{\rm K}^*(892)^0$ meson throughout the text. The kinematic region of these measurements is $p_{\rm T}<20$ GeV/c and $2.0<y<4.5$ for the b hadron. The production ratio of the two b hadrons, defined as

$$R_{\Lambda_{\rm b}^0/\overline{\rm B}^0}\equiv\frac{\sigma(\Lambda_{\rm b}^0)\mathcal{B}(\Lambda_{\rm b}^0\to {\rm J/\psi\, pK^-})}{\sigma(\overline{\rm B}^0)\mathcal{B}(\overline{\rm B}^0\to {\rm J/\psi}\overline{\rm K}^{*0})}, \tag{1}$$

is determined, taking advantage of the cancellation of some uncertainties in both experimental measurements and theoretical calculations. Here, $\sigma(\Lambda_{\rm b}^0)$ and $\sigma(\overline{\rm B}^0)$ represent the production cross-sections of $\Lambda_{\rm b}^0$ and $\overline{\rm B}^0$ hadrons in pp collisions. The branching fraction $\mathcal{B}(\Lambda_{\rm b}^0\to {\rm J/\psi\, pK^-})$ is calculated from this result using previous measurements of $f_{\Lambda_{\rm b}^0}/f_{\rm d}$ [7, 8] and $\mathcal{B}(\overline{\rm B}^0\to {\rm J/\psi}\overline{\rm K}^{*0})$ [12]. The kinematic dependence of the sum of the asymmetries in the production and decay, $a_{\rm p+d}\equiv a_{\rm prod}+a_{\rm decay}$, between $\Lambda_{\rm b}^0$ and $\overline{\Lambda}_{\rm b}^0$ is studied using $\Lambda_{\rm b}^0\to {\rm J/\psi\, pK^-}$ and $\Lambda_{\rm b}^0\to {\rm J/\psi}\,\overline{\rm p}{\rm K}^+$ decays. Furthermore, using the measurement of $\mathcal{B}(\Lambda_{\rm b}^0\to {\rm J/\psi\, pK^-})$, the branching fractions of the decays $\Lambda_{\rm b}^0\to {\rm J/\psi\, p\pi^-}$ and $\Lambda_{\rm b}^0\to {\rm P_c^+}(\to {\rm J/\psi\, p}){\rm K^-}$ are determined.

The measurements in this paper are based on a data sample corresponding to an integrated luminosity of $3\,{\rm fb}^{-1}$, collected by the LHCb experiment in pp collisions at centre-of-mass energies $\sqrt{s}=7$ TeV in 2011 and $\sqrt{s}=8$ TeV in 2012. Separate measurements are performed for each of the two centre-of-mass energies.

2 Detector and simulation

The LHCb detector [13, 14] is a single-arm forward spectrometer covering the pseudorapidity range $2<\eta<5$, designed for the study of particles containing b or c quarks. The detector includes a high-precision tracking system consisting of a silicon-strip vertex detector surrounding the pp interaction region [15], a large-area silicon-strip detector located upstream of a dipole magnet with a bending power of about 4 Tm, and three stations of silicon-strip detectors and straw drift tubes [16] placed downstream of the magnet. The tracking system provides a measurement of momentum, p, of charged particles with a relative uncertainty that varies from 0.5% at low momentum to 1.0% at 200 GeV/c. The minimum distance of a track to a primary vertex (PV), the impact parameter (IP), is measured with a resolution of $(15+29/p_{\rm T})\mu$m, where $p_{\rm T}$ is the component of the momentum transverse to the beam, in GeV/c. Different types of charged hadrons are distinguished using information from two ring-imaging Cherenkov detectors [17]. Photons, electrons and hadrons are identified by a calorimeter system consisting of scintillating-pad and preshower detectors, an electromagnetic calorimeter and a hadronic calorimeter. Muons are identified by a system composed of alternating layers of iron and multiwire proportional chambers [18]. The online event selection is performed by a trigger [19], which consists of a hardware stage, based on information from the calorimeter and muon systems, followed by a software stage, which applies a full event reconstruction. In the hardware trigger, events are selected by requiring at least one high-$p_{\rm T}$ track that is consistent with a muon hypothesis. In the software trigger, two well-reconstructed muons are required to form a vertex with good fit χ^2 and to have an invariant mass consistent with that of the J/ψ meson [20]. The trigger also requires a significant displacement between the J/ψ vertex and the associated PV of the pp collision.

In the simulation, pp collisions are generated using Pythia [21, 22] with a specific LHCb configuration [23]. Decays of hadronic particles are described by EvtGen [24], in which final-state radiation is generated using Photos [25]. The interaction of the generated particles with the detector, and its response, are implemented using the Geant4 toolkit [26, 27] as described in Ref. [28]. The physics models used by LHCb in Geant4 for hadronic interactions have been tested against experimental data from COMPAS [20], and good agreement was observed.*

3 Event selection

Candidates for $\Lambda_{\rm b}^0$ ($\overline{\rm B}^0$) hadrons are reconstructed in the $\Lambda_{\rm b}^0\to {\rm J/\psi\, pK^-}$ ($\overline{\rm B}^0\to {\rm J/\psi}\overline{\rm K}^{*0}$) decay channel, where the J/ψ mesons are reconstructed in the dimuon final state, and $\overline{\rm K}^{*0}$ candidates are reconstructed from $\overline{\rm K}^{*0}\to {\rm K^-}\pi^+$ decays. Since the $\Lambda_{\rm b}^0\to {\rm J/\psi\, pK^-}$ and $\overline{\rm B}^0\to {\rm J/\psi}\overline{\rm K}^{*0}$ decays have the same topology, a similar event selection is adopted for both.

An offline selection is applied after the trigger and is divided into two steps: a preselection and a multivariate selection based on a boosted decision tree (BDT) [29–32].

*Data files are courtesy of the COMPAS Group, IHEP, Protvino, Russia.

In the preselection, each track of the Λ_b^0 ($\overline{B}^0$) candidate is required to be of good quality [14, 33–35]. Identified muons are required to have p_T greater than 550 MeV/c, while hadrons are required to have p_T greater than 250 MeV/c. The muons should be inconsistent with originating from any PV, as determined by their impact parameter. Each J/ψ candidate is required to have a good vertex fit χ^2 and an invariant mass within $^{+43}_{-48}$MeV/c^2 of the known J/ψ mass [20]. Particle identification (PID) requirements are imposed on the final-state tracks. For the kaon and proton in the $\Lambda_b^0 \to J/\psi p K^-$ decay, the sum of the kaon and proton p_T should be larger than 1 GeV/c. Each $\overline{K}^{*0}$ candidate is required to have a good vertex fit χ^2 and to have p_T greater than 1 GeV/c. The invariant mass of the reconstructed $\overline{K}^{*0}$ is required to be within ±70 MeV/c^2 of the $\overline{K}^{*0}$ mass [20]. Each b hadron candidate must have a good vertex fit χ^2, be consistent with originating from the PV, and have a decay time greater than 0.2 ps.

Some non-combinatorial backgrounds exist in the $\Lambda_b^0 \to J/\psi p K^-$ data sample, originating from $\overline{B}^0 \to J/\psi K^-\pi^+$ and $\overline{B}_s^0 \to J/\psi K^- K^+$ decays with the π^+ and K^+ misidentified as a proton. In order to suppress these events, the invariant mass is recalculated by interpreting the proton candidate as a pion or a kaon, and the two relevant invariant mass regions are vetoed: $m(J/\psi K^-\pi^+) \in [5250,5310]$ MeV/c^2 and $m(J/\psi K^+K^-) \in [5340,5400]$ MeV/c^2. After the mass vetoes these background contributions are reduced to a negligible level.

After the preselection, the $\Lambda_b^0 \to J/\psi p K^-$ ($\overline{B}^0 \to J/\psi \overline{K}^{*0}$) candidates are filtered with the BDT to further suppress combinatorial background. For the decays $\Lambda_b^0 \to J/\psi p K^-$ and $\overline{B}^0 \to J/\psi \overline{K}^{*0}$, the same BDT classifier is applied. Independent BDT classifiers are used for the 2011 and 2012 samples. In the BDT training a simulated Λ_b^0 sample is used as the signal. The background is taken from the lower, (5420,5560) MeV/c^2, and upper, (5680,5820) MeV/c^2, sidebands of the Λ_b^0 invariant mass distribution in data. Events in the sidebands are randomly divided into two parts, one for the training and the other for the test. No overtraining is observed. The following information is used by the BDT classifier: the kinematic properties and the impact parameters of the tracks; and the vertex quality, the decay length and the impact parameter of the reconstructed b hadron candidate. The variables used for the training are chosen based on their power to discriminate signal from background and on the similarity of their distributions for $\Lambda_b^0 \to J/\psi p K^-$ and $\overline{B}^0 \to J/\psi \overline{K}^{*0}$ decays. The threshold for the BDT response is chosen to maximise $S/\sqrt{S+B}$, where B represents the number of background events estimated from the sideband region and S the number of signal events in the mass peak.

4 Cross-section and branching fraction determination

The product of the differential production cross-section of each b hadron and the corresponding branching fraction is calculated as

$$\frac{\mathrm{d}^2\sigma}{\mathrm{d}p_T\,\mathrm{d}y}\,\mathcal{B} = \frac{N(p_T,y)}{\varepsilon(p_T,y)\;\mathcal{L}\;\mathcal{B}_{\rm inter}\,\Delta p_T\,\Delta y}, \tag{2}$$

where $N(p_T,y)$ and $\varepsilon(p_T,y)$ are respectively the signal yield and the efficiency as functions of p_T and y of the b hadron, Δp_T and Δy are the bin widths, $\mathcal{L}$ is the integrated luminosity, $\mathcal{B}$ is the absolute branching fraction of the $\Lambda_b^0 \to J/\psi p K^-$ ($\overline{B}^0 \to J/\psi \overline{K}^{*0}$) decay, and $\mathcal{B}_{\rm inter}$ represents the branching fractions of the intermediate decays:

$$\mathcal{B}_{\rm inter} \equiv \begin{cases} \mathcal{B}(J/\psi \to \mu^+\mu^-) & \text{for } \Lambda_b^0, \\ \mathcal{B}(J/\psi \to \mu^+\mu^-)\;\mathcal{B}(\overline{K}^{*0} \to K^-\pi^+) & \text{for } \overline{B}^0. \end{cases}$$

The luminosity is measured with van der Meer scans and a beam-gas imaging method [36]. The 2011 and 2012 data samples correspond to 1019±17 pb^{-1} and 2056±23 pb^{-1}, respectively. The branching fraction $\mathcal{B}(J/\psi \to \mu^+\mu^-) = (5.961\pm0.033)\%$ [20], while $\mathcal{B}(\overline{K}^{*0} \to K^-\pi^+)$ is taken to be 2/3 assuming isospin symmetry. The branching fraction $\mathcal{B}(\overline{B}^0 \to J/\psi \overline{K}^{*0}) = (1.29\pm0.05\pm0.13)\times10^{-3}$ as measured by Belle [12] is used in preference to the world average value, since in the Belle result the S-wave component is subtracted.

5 Signal determination

The signal yields of the $\Lambda_b^0 \to J/\psi p K^-$ and $\overline{B}^0 \to J/\psi \overline{K}^{*0}$ decays are determined from unbinned extended maximum likelihood fits to the invariant mass distributions of the reconstructed b hadron candidates in each p_T and y bin. In order to improve the mass resolution, the b hadron is refitted with constraints [37] that it originates from the PV and that the reconstructed J/ψ mass equals its known mass [20].

Figure 1 shows, as an example of one of the fit results, the invariant mass distributions of Λ_b^0 and $\overline{B}^0$ candidates in the kinematic region $p_T \in [6,7]$ GeV/c and $y \in [3.0,3.5]$ for the 2012 data sample. The signal shape in the fits is modelled by a double-sided Crystal Ball (DSCB) function, an empirical function comprising a Gaussian core together with power-law tails on both sides. The mean and the mass resolution of the DSCB function are free in the fits, while the tail parameters are determined from simulation in each kinematic bin according to the empirical function given in Ref. [38]. The combinatorial background is modelled by an exponential function whose parameters are left free in the fits.

In the fits to the Λ_b^0 mass distribution, there is a contribution from the $\Lambda_b^0 \to J/\psi p K^-$ decay in which the proton is misidentified as a kaon and the kaon is misidentified as a proton. This background is denoted as the doubly misidentified background, and it is modelled by a DSCB function. All parameters of this DSCB function are fixed from the simulation study, including: the difference between the mean of this DSCB function and that of the signal shape; the ratio of the mass resolution between these two DSCB; the yield fraction relative to the Λ_b^0 signal channel; and the tail parameters.

In the $\overline{B}^0 \to J/\psi \overline{K}^{*0}$ sample, in addition to the combinatorial background, there are two further sources of background. One is the decay $\overline{B}_s^0 \to J/\psi \overline{K}^{*0}$, which populates the upper sideband of the invariant mass distribution, and is modelled with a DSCB function. The tail parameters of this DSCB function are the same as those of the $\overline{B}^0$ signal shape and the remaining parameters are free in the fits. The other comes from partially reconstructed B mesons and is described by the tail of a Gaussian function. The associated mean and width are free parameters in the fits.

According to a previous LHCb measurement [39], the fraction of the $\overline{K}^{*0}$ meson contribution in the $\overline{B}^0 \to J/\psi \overline{K}^{*0}$ decay is calculated as $(89.9\pm0.4\pm1.3)\%$, where the remainder is due to the S-wave component in the $K^-\pi^+$ system and its interference with the $\overline{K}^{*0}$ meson. The fitted $\overline{B}^0$ yields are subtracted with this number to remove the components from S-wave and its interference.

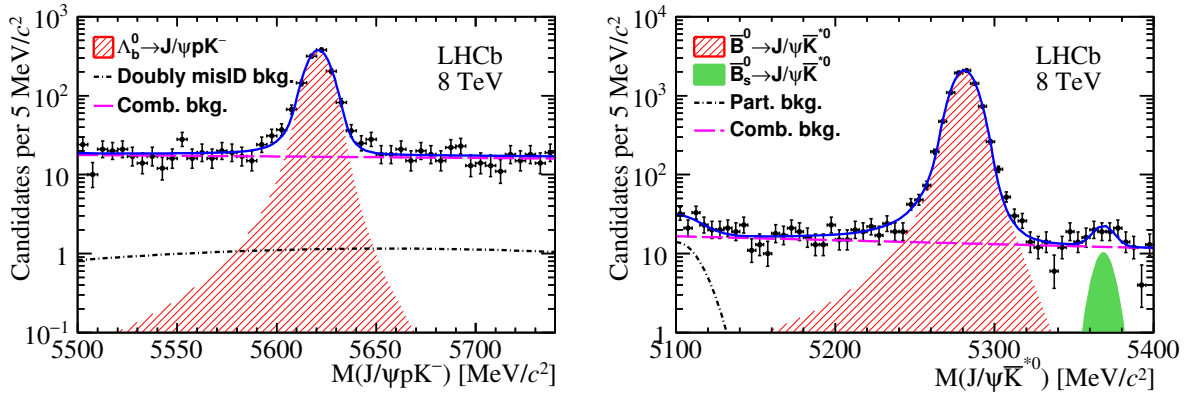

Fig. 1. (color online) Fit to the (left) $J/\psi pK^-$ and (right) $J/\psi \overline{K}^{*0}$ invariant mass distributions with $p_T \in [6,7]$ GeV/c and $y \in [3.0,3.5]$ for the 2012 data sample. The hatched (red) area represents the signals, the filled (green) area $\overline{B}_s^0 \to J/\psi \overline{K}^{*0}$, and the dashed (magenta) lines the combinatorial background. The dot-dashed (black) lines indicate the doubly misidentified background (left) and partially reconstructed background (right). The solid (blue) lines represent the sum of the above components and the points with error bars show the data.

6 Efficiencies

The efficiency $\varepsilon^{\Lambda_b^0,\overline{B}^0}(p_T,y)$ consists of the geometrical acceptance of the detector, the trigger efficiency, the reconstruction and preselection efficiency, the hadron PID efficiency, and the BDT selection efficiency. All the efficiencies are determined from a sample of simulated signal events, except the hadron PID efficiency, which is determined from data with tracks from the decays $J/\psi \to \mu^+\mu^-$, $D^{*+} \to D^0(\to K^-\pi^+)\pi^+$ and $\Lambda_c^+ \to pK^-\pi^+$.

The rich resonance structure observed in decays of $\Lambda_b^0 \to J/\psi p K^-$ in data [10] is not modelled in the simulation. The simulated sample is weighted to reproduce the distributions of the BDT training variables and the two-dimensional distribution of $m(pK^-)$ and $m(J/\psi p)$ observed in the background-subtracted data sample, which has been obtained using the *sPlot* technique [40], with the b-hadron invariant mass as the discriminating variable. It is found that the correlations between the discriminating variable and the control variables are negligible.

7 Asymmetry determination

The observed (raw) asymmetry for Λ_b^0 and $\overline{\Lambda}_b^0$ is defined as

$$A_{raw}(x) \equiv \frac{N^{\Lambda_b^0}(x) - N^{\overline{\Lambda}_b^0}(x)}{N^{\Lambda_b^0}(x) + N^{\overline{\Lambda}_b^0}(x)}. \quad (3)$$

The symbol $N(x)$ is the signal yield in the given bin of x from the fits to the invariant mass distribution of the Λ_b^0 ($\overline{\Lambda}_b^0$) sample, where x denotes p_T or y. The observed asymmetry is a sum of several contributions: the asymmetry between the numbers of the produced Λ_b^0 and $\overline{\Lambda}_b^0$ baryons in pp collisions, $a_{prod}(x)$; the decay asymmetry between the $\Lambda_b^0 \to J/\psi p K^-$ and $\Lambda_b^0 \to J/\psi \overline{p} K^+$ channels, $a_{decay}(x)$; the asymmetry between the p and $\overline{p}$ detec-

tion efficiencies, $a_{\rm D}^{\rm p}(x)$; the asymmetry between the $\rm K^-$ and $\rm K^+$ detection efficiencies, $a_{\rm D}^{\rm K}(x)$; and the asymmetry between the PID efficiencies for $\Lambda_{\rm b}^0$ and $\overline{\Lambda}_{\rm b}^0$ baryons, $a_{\rm PID}(x)$. Other possible asymmetries are neglected. Assuming that all these asymmetries are small, the asymmetries $a_{\rm p+d}(x)$ of $\Lambda_{\rm b}^0$ and $\overline{\Lambda}_{\rm b}^0$ baryons can be calculated as

$$a_{\rm p+d}(x)=A_{\rm raw}(x)-a_{\rm PID}(x)-a_{\rm D}^{\rm p}(x)-a_{\rm D}^{\rm K}(x). \quad (4)$$

The value $A_{\rm raw}(x)-a_{\rm PID}(x)$ can be calculated as

$$A_{\rm raw}(x)-a_{\rm PID}(x)=\frac{N^{\Lambda_{\rm b}^0}(x)/\varepsilon_{\rm PID}^{\Lambda_{\rm b}^0}(x)-N^{\overline{\Lambda}_{\rm b}^0}(x)/\varepsilon_{\rm PID}^{\overline{\Lambda}_{\rm b}^0}(x)}{N^{\Lambda_{\rm b}^0}(x)/\varepsilon_{\rm PID}^{\Lambda_{\rm b}^0}(x)+N^{\overline{\Lambda}_{\rm b}^0}(x)/\varepsilon_{\rm PID}^{\overline{\Lambda}_{\rm b}^0}(x)}, \quad (5)$$

where $\varepsilon_{\rm PID}^{\Lambda_{\rm b}^0}(x)$ and $\varepsilon_{\rm PID}^{\overline{\Lambda}_{\rm b}^0}(x)$ represent the PID efficiencies for $\Lambda_{\rm b}^0$ and $\overline{\Lambda}_{\rm b}^0$. The kaon detection asymmetry $a_{\rm D}^{\rm K}(x)$ as a function of $p_{\rm T}$ and y is obtained from a previous LHCb study [41]. The proton detection asymmetry $a_{\rm D}^{\rm p}(x)$ as a function of $p_{\rm T}$ or y is estimated from simulation, which uses the GEANT4 model as described in Section 2. The proton detection asymmetry as a function of $p_{\rm T}$ or y is calculated with the proton and antiproton track reconstruction efficiencies in the corresponding kinematic bin. It is checked that the kinematic distributions of protons and $\Lambda_{\rm b}^0$ baryons in the simulation sample are consistent with those in the data sample. As a crosscheck, the proton detection asymmetries are also estimated through a simulation sample, where the $\Lambda_{\rm b}^0$ signals are partially reconstructed without using the proton information, and the results are consistent.

8 Systematic uncertainties

Several sources of systematic uncertainties are studied in the analysis and are summarised in Tables 1 and 2. For the production cross-section measurements, the uncertainties originate from the determination of the signal yields, efficiencies, branching fractions and luminosities. The total systematic uncertainties are obtained from the sum in quadrature of all components.

Imperfect knowledge of the mass distributions for the signal and backgrounds causes systematic uncertainties in the signal yield determination. For the signal shape, the Apollonios function [42] and the sum of a Gaussian function and a Crystal Ball function are tried as alternatives to the DSCB. The largest deviation to the nominal result is taken as the uncertainty due to the model of the signal shape.

The fits are repeated with a linear function substituted for the exponential model for the combinatorial background. The fits are also repeated without the double misidentified components. The maximum differences of the signal yields from the nominal results are quoted as systematic uncertainties due to the background shape.

Table 1. Summary of the systematic uncertainties (%) for the production cross-sections of $\Lambda_{\rm b}^0$ and $\overline{\rm B}^0$. The large uncertainties affect the bins with very few candidates.

	$\Lambda_{\rm b}^0$ (7 TeV)	$\Lambda_{\rm b}^0$ (8 TeV)	$\overline{\rm B}^0$ (7 TeV)	$\overline{\rm B}^0$ (8 TeV)
Uncorrelated between bins				
Signal shape	0.4−15.4	0.2− 6.2	0.2−1.5	0.2− 1.5
Background shape	0.0− 1.9	0.0− 4.3	0.0−0.9	0.0− 0.9
Simulation sample size	4.1−16.5	3.9−14.3	1.7−9.5	2.2−14.9
BDT efficiency	0.4− 2.5	0.4− 2.8	0.1−0.5	0.1− 0.5
Trigger efficiency	0.0− 4.6	0.0−14.9	0.0−2.1	0.0− 4.0
PID efficiency	0.4− 8.4	0.4−15.8	0.2−4.6	0.2− 2.7
Resonance			0.0−1.0	0.0− 1.8
Correlated between bins				
Tracking efficiency	3.0	3.0	3.0	3.0
Mass veto efficiency	1.3	1.9		
Luminosity	1.7	1.2	1.7	1.2
$\mathcal{B}(\rm J/\psi\to\mu^+\mu^-)$	0.6	0.6	0.6	0.6
S-wave and interference in $\rm K^-\pi^+$			1.4	1.4

Table 2. Summary of the absolute systematic uncertainties (%) for the asymmetry of $\Lambda_{\rm b}^0$ and $\overline{\Lambda}_{\rm b}^0$. The large uncertainties affect the bins with very few candidates.

	2011	2012
PID efficiency	0.4−4.4	0.0−2.6
Signal shape	0.0−0.8	0.0−0.9
Background shape	0.0−0.1	0.0−0.3
MC statistics	0.7−5.4	0.3−4.2
Tracking asymmetry of proton	0.1−1.9	0.1−1.9

Most efficiencies are estimated from simulation. The limited size of the simulation sample leads to systematic uncertainties on the efficiencies ranging from 1.7% to 16.5%.

The tracking efficiency is estimated from simulation and calibrated by data [43]. The uncertainty of the calibration is 0.4% per track. Additional systematic uncertainties are assigned to hadrons due to imperfect knowledge of hadron interactions in the detector, 1.1% for kaons, 1.4% for pions and 1.4% for protons.

The BDT efficiency is estimated with the weighted simulation sample to ensure that the distributions of the two training variables, the kinematic properties of the tracks and the vertex quality, agree with those in data. The uncertainties on the weights are propagated to the final results to give the corresponding systematic uncertainty.

The trigger efficiency is determined in the simulation and validated in a control sample of $J/\psi \to \mu^+\mu^-$ decays [19]. The difference of the central values of this determination in data and the simulation in each bin is taken as the systematic uncertainty. Uncertainties due to the limited sample size of the simulation are added in quadrature.

The PID efficiency is estimated with a data-driven method. A sample of $J/\psi \to \mu^+\mu^-$, $D^{*+} \to D^0(\to K^-\pi^+)\pi^+$ and $\Lambda_c^+ \to pK^-\pi^+$ decays obtained without using PID information is used to evaluate the PID efficiency. The limited sample size used to calculate the PID efficiency introduces a systematic uncertainty in each kinematic bin. To study the bin-by-bin migration effect, the number of the bins is doubled or halved and the PID efficiency is recalculated. The largest deviation from the nominal result is taken as the uncertainty.

To account for the rich and complex structure of multiple intermediate resonances in the $\Lambda_b^0 \to J/\psi\, pK^-$ decay, the simulation sample is weighted in two-dimensional bins of $m(K^-p)$ and $m(J/\psi p)$ to match the data. Pseudoexperiments are performed to estimate the systematic uncertainties due to the weights. The weight in each bin is varied according to its uncertainty and the total efficiency is recalculated. The RMS of the distribution obtained from the pseudoexperiments is taken as the systematic uncertainty. As mentioned in Section 3, the preselection includes mass vetoes. The preselection efficiencies are estimated from the simulation sample. A fit to the Λ_b^0 invariant mass distribution in the vetoed data sample is performed, which gives the number of $\Lambda_b^0 \to J/\psi\, pK^-$ signal events rejected by the vetoes. The fraction of the vetoed signal events in the data sample is compared with that in the simulation sample. A difference of 1.3% (1.9%) is observed for the 2011 (2012) sample, and this is taken as the systematic uncertainty.

The uncertainty in the determination of the integrated luminosity is 1.7% (1.2%) for the 2011 (2012) data sample [36]. An uncertainty of 0.6% is taken on $\mathcal{B}(J/\psi \to \mu^+\mu^-)$ [20]. The fractions of the S-wave component in the $K^-\pi^+$ system and their interference were determined by a previous LHCb measurement, and their 1.4% uncertainty [39] is taken as a systematic uncertainty for the $\overline{B}^0 \to J/\psi \overline{K}^{*0}$ decay.

In the Λ_b^0 and $\overline{\Lambda}_b^0$ asymmetry measurement, all of the uncertainties mentioned above cancel in the ratio, except for those due to the signal shape, the background shape, the limited sample size and the PID efficiency. Since a data-driven determination of proton detection asymmetries is not available, the difference in the determination of the kaon detection asymmetries in data and simulation is taken as a systematic uncertainty for the proton detection asymmetry. The uncertainties vary from 0.1% to 1.9% in kinematic bins, with large values occurring in bins of low p_T or low signal yields. In the LHCb GEANT4 physics models, the cross-sections of interactions between particles and the material are checked with test beam data as discussed in Section 2. There are more data for protons than for kaons. Therefore, these uncertainties can be considered to be conservative.

9 Cross-section results

The product of the Λ_b^0 ($\overline{B}^0$) double-differential cross-section and the branching fraction of the decay $\Lambda_b^0 \to J/\psi\, pK^-$ ($\overline{B}^0 \to J/\psi \overline{K}^{*0}$) is shown in Fig. 2, and the values are listed in Tables 3, 4, 5 and 6 in the Appendix. By integrating over y or p_T, the single differential production cross-sections, shown in Fig. 3, are obtained. Figure 4 shows the p_T distribution of the Λ_b^0 production, fitted by a power-law function with the Tsallis parameterisation [44, 45]:

$$\frac{\mathrm{d}\sigma}{p_T \mathrm{d}p_T} \propto \frac{1}{[1+E_{k\perp}/(TN)]^N}, \tag{6}$$

where T is a temperature-like parameter, N determines the power-law behaviour at large $E_{k\perp}$, and $E_{k\perp} \equiv \sqrt{p_T^2+M^2}-M$ with M the mass of the hadron. The fit results are

$$T=1.12\pm0.04 \text{ GeV} \qquad N=7.3\pm0.5 \qquad (7 \text{ TeV}),$$
$$T=1.13\pm0.03 \text{ GeV} \qquad N=7.5\pm0.4 \qquad (8 \text{ TeV}).$$

For the 7 TeV (8 TeV) sample, the fit χ^2 is 21.0 (10.7) for 7 (9) degrees of freedom. The parameters T and N obtained from the 7 TeV and 8 TeV samples are consistent with each other and with the values found by CMS [5]. Other functions suggested in Ref. [46] do not give acceptable fits to the data. In Fig. 4 the data points are placed in the bin according to the prescription of Ref. [47].

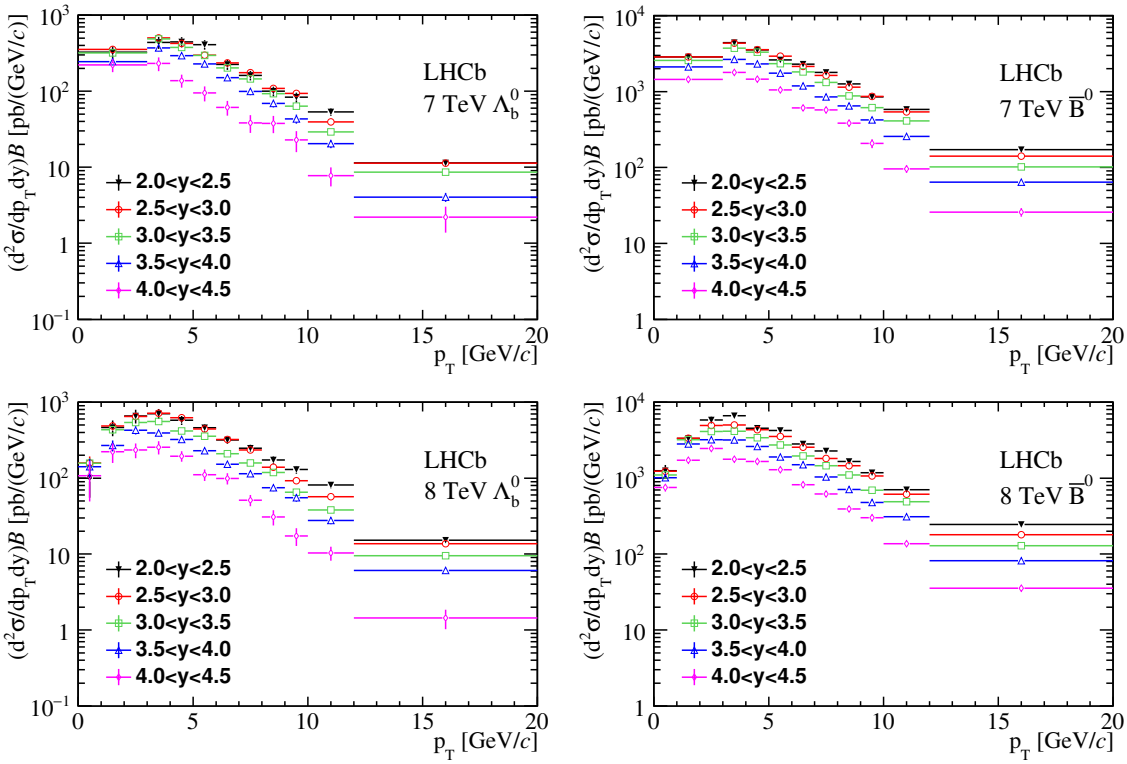

Fig. 2. (color online) Products of production cross-sections and branching fractions as functions of p_T in y bins for (left) $\Lambda_b^0 \to J/\psi p K^-$ and (right) $\overline{B}^0 \to J/\psi \overline{K}^{*0}$. The top (bottom) plots represent the 2011 (2012) sample. The error bars represent the total uncertainties.

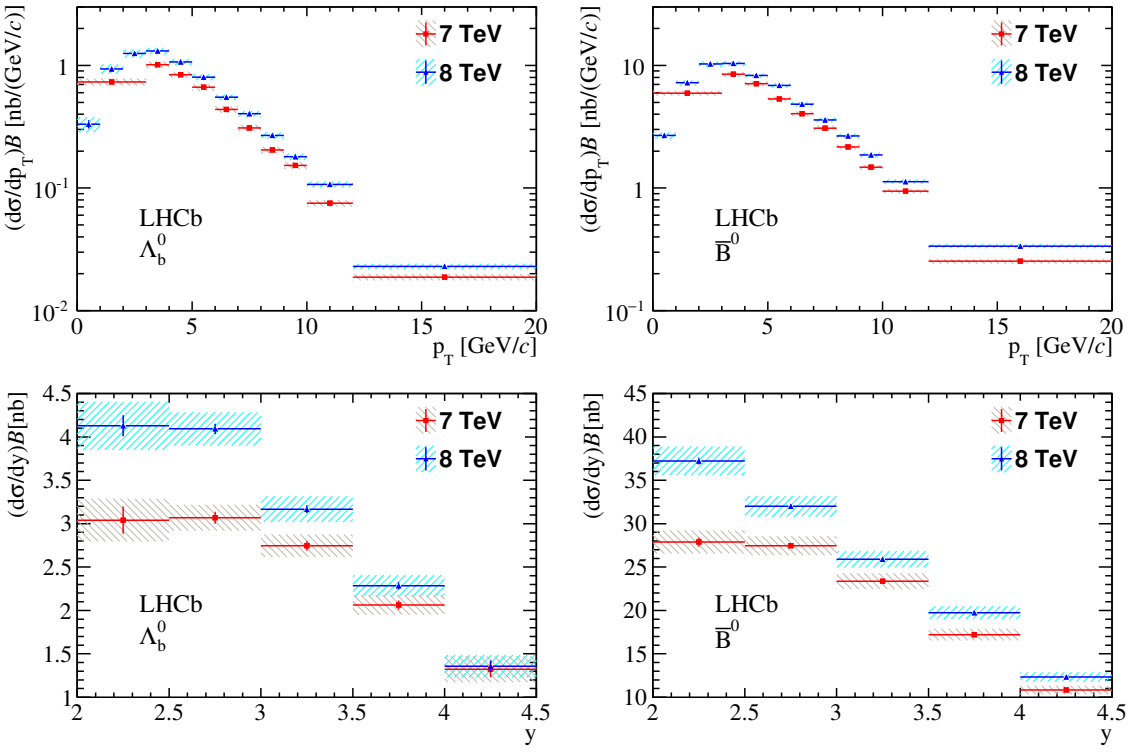

Fig. 3. (color online) Products of production cross-sections and branching fractions as functions of (top) p_T or (bottom) y. The left (right) plots represent Λ_b^0 ($\overline{B}^0$) hadrons. The error bars indicate the statistical uncertainties and the hatched areas represent the total uncertainties.

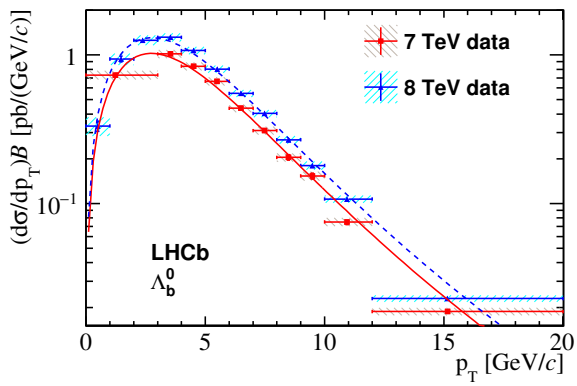

Fig. 4. (color online) Fit to the Λ_b^0 distribution with the Tsallis function.

The integrated cross-sections of the b hadrons with $0<p_T<20$ GeV/c and $2.0<y<4.5$ are measured to be

$$\begin{aligned}
&\sigma(\Lambda_b^0,\ \sqrt{s}=7\ \text{TeV})\ \mathcal{B}(\Lambda_b^0\to J/\psi\, pK^-)\\
&=6.12\pm0.10(\text{stat})\pm0.25(\text{syst})\ \text{nb},\\
&\sigma(\Lambda_b^0,\ \sqrt{s}=8\ \text{TeV})\ \mathcal{B}(\Lambda_b^0\to J/\psi\, pK^-)\\
&=7.51\pm0.08(\text{stat})\pm0.31(\text{syst})\ \text{nb},\\
&\sigma(\overline{B}^0,\ \sqrt{s}=7\ \text{TeV})\ \mathcal{B}(\overline{B}^0\to J/\psi\overline{K}^{*0})\\
&=53.4\pm0.3\ (\text{stat})\pm2.0\ (\text{syst})\ \text{nb},\\
&\sigma(\overline{B}^0,\ \sqrt{s}=8\ \text{TeV})\ \mathcal{B}(\overline{B}^0\to J/\psi\overline{K}^{*0})\\
&=63.6\pm0.2\ (\text{stat})\pm2.3\ (\text{syst})\ \text{nb}.
\end{aligned}$$

Taking the branching fraction $\mathcal{B}(\overline{B}^0\to J/\psi\overline{K}^{*0})$ from Belle [12], the measured $\overline{B}^0$ production cross-section at 7 TeV is consistent with the previous LHCb measurement [38]. The ratios of the Λ_b^0 and $\overline{B}^0$ integrated production cross-sections between 8 TeV and 7 TeV, in the kinematic range $0<p_T<20$ GeV/c and $2.0<y<4.5$, are

$$\frac{\sigma(\sqrt{s}=8\ \text{TeV})}{\sigma(\sqrt{s}=7\ \text{TeV})}=\begin{cases}1.23\pm0.02\pm0.04 & \text{for } \Lambda_b^0,\\ 1.19\pm0.01\pm0.02 & \text{for } \overline{B}^0,\end{cases}$$

where the first uncertainties are statistical and the second systematic. Many systematic uncertainties cancel totally or partially in these ratios: the ratio of the luminosities is known with a precision of 1.44% [36]; the tracking efficiency is considered to be fully correlated, due to the fact that the associated systematic uncertainty is dominated by hadronic interactions of the tracks in the detector; the mass veto efficiency, the branching fraction of the $J/\psi\to\mu^+\mu^-$ decay, and the S-wave contribution in the $K^-\pi^+$ system are also fully correlated. All other sources are considered uncorrelated. The ratio of the integrated production cross-sections agrees with FONLL predictions [48–50]. Figure 5 shows the p_T and y dependence of the ratios for Λ_b^0 and $\overline{B}^0$ production cross-sections at 8 TeV with respect to those at 7 TeV, together with linear fits to the distributions:

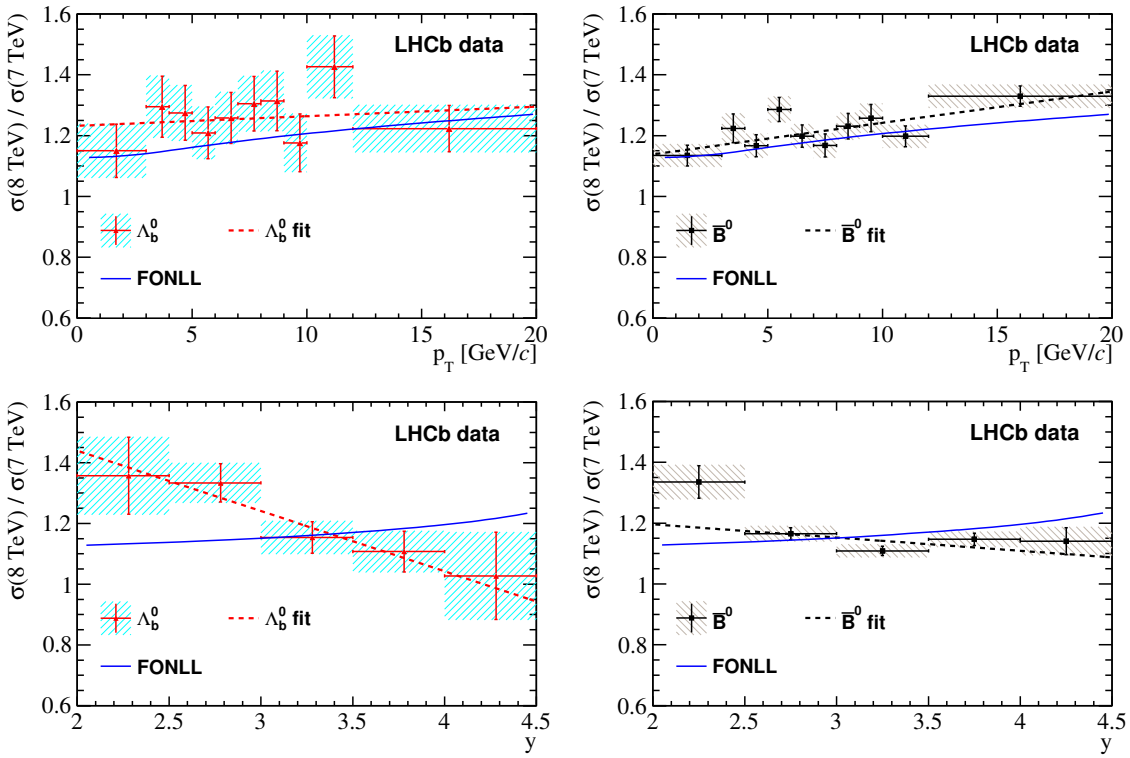

Fig. 5. (color online) Production ratios of (left) Λ_b^0 and (right) $\overline{B}^0$ at 8 TeV and 7 TeV as functions of the (top) p_T and (bottom) y of the b hadron. The blue lines are FONLL predictions. The error bars represent uncorrelated uncertainties, while the hatched areas show the total uncertainties. Linear fits are also shown.

$$\Lambda_b^0 \begin{cases} (1.25\pm0.03)+(0.003\pm0.007)(p_T-\langle p_T\rangle)/(\mathrm{GeV}/c) & \chi^2/\mathrm{ndf}=6.1/8, \\ (1.22\pm0.03)-(0.20\pm0.07)(y-\langle y\rangle) & \chi^2/\mathrm{ndf}=1.2/3, \end{cases}$$

$$\overline{\mathrm{B}}^0 \begin{cases} (1.21\pm0.01)+(0.010\pm0.003)(p_T-\langle p_T\rangle)/(\mathrm{GeV}/c) & \chi^2/\mathrm{ndf}=12/8, \\ (1.15\pm0.01)-(0.04\pm0.02)(y-\langle y\rangle) & \chi^2/\mathrm{ndf}=15/3, \end{cases}$$

where $\langle p_T\rangle=6.7$ (6.9) GeV/c is the mean p_T of Λ_b^0 ($\overline{\mathrm{B}}^0$) hadrons in the data sample, $\langle y\rangle=3.1$ is the mean y, and ndf is the number of degrees of freedom. The p_T dependence of the ratio agrees with FONLL predictions, while the y dependence does not.

The measured values of the ratio $R_{\Lambda_b^0/\overline{\mathrm{B}}^0}$, defined in Eq. (1), as a function of p_T and y are shown in Fig. 6. In the region $p_T<5$ GeV/c, no p_T dependence of the ratio $R_{\Lambda_b^0/\overline{\mathrm{B}}^0}$ is observed, while the ratio decreases for $p_T>5$ GeV/c. No dependence with rapidity is observed. In Fig. 6 the p_T dependence of the ratio $R_{\Lambda_b^0/\overline{\mathrm{B}}^0}$ is fitted with the fragmentation function ratio $f_{\Lambda_b^0}/f_d(p_T)$ given in Ref. [8], which is only defined in the range $p_T>3$ GeV/c.

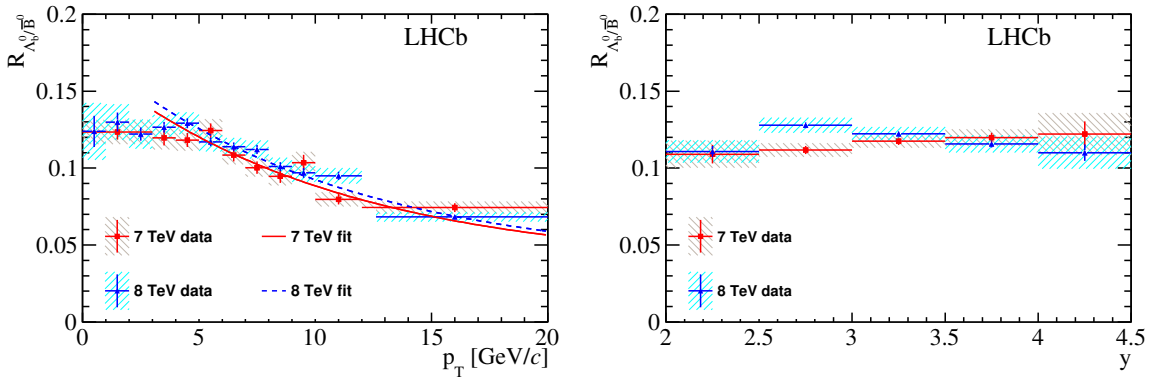

Fig. 6. (color online) Ratio $R_{\Lambda_b^0/\overline{\mathrm{B}}^0}$ as a function of (left) p_T and (right) y for the 2011 and 2012 samples, where the error bars indicate statistical uncertainties and the hatched areas the total uncertainties. The red solid (blue dashed) line in the left plot represents the fit to the ratio $f_{\Lambda_b^0}/f_d(p_T)$ from Ref. [8] for the 2011 (2012) data sample.

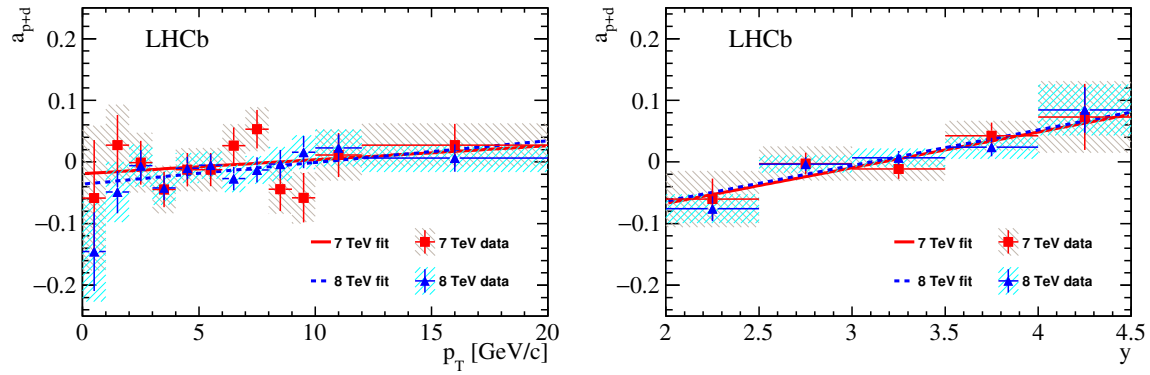

Fig. 7. (color online) Asymmetries a_{p+d} between Λ_b^0 and $\overline{\Lambda}_b^0$ as functions of (left) p_T and (right) y. The error bars indicate statistical uncertainties, and the hatched areas the total uncertainties.

The asymmetry a_{p+d} between Λ_b^0 and $\overline{\Lambda}_b^0$ is shown in Fig. 7. The values are listed in Table 7 in the Appendix. The data points are fitted with linear functions. The slope fitted to the asymmetry as a function of p_T is consistent with zero, $(2.3\pm3.0)\times10^{-3}/(\mathrm{MeV}/c)$ for 7 TeV and $(3.5\pm2.0)\times10^{-3}/(\mathrm{MeV}/c)$ for 8 TeV. The fit to $a_{p+d}(y)$ gives a non-zero slope, and a combination of the results for 7 TeV and 8TeV gives

$$a_{p+d}(y)=(-0.001\pm0.007)+(0.058\pm0.014)(y-\langle y\rangle),$$

where $\langle y\rangle=3.1$ is the average rapidity of Λ_b^0 hadrons in the data sample. The non-zero slope suggests some

baryon number transport from the beam particles to the less centrally produced Λ_b^0, which leads to a $\Lambda_b^0/\overline{\Lambda}_b^0$ cross-section ratio that increases with rapidity and which can be interpreted as, for example, a string drag effect or leading quark effect [6, 51].

10 Branching fraction results

The ratio $R_{\Lambda_b^0/\overline{B}^0}$ can be calculated in bins of p_T as:

$$R_{\Lambda_b^0/\overline{B}^0}(p_T)=\frac{N_{sig}^{\Lambda_b^0}(p_T)\varepsilon_{tot}^{\overline{B}^0}(p_T)}{N_{sig}^{\overline{B}^0}(p_T)\varepsilon_{tot}^{\Lambda_b^0}(p_T)}\,\mathcal{B}(\overline{K}^{*0}\to K^-\pi^+). \quad (7)$$

It is related to the fragmentation fraction ratio $f_{\Lambda_b^0}/f_d$ through

$$R_{\Lambda_b^0/\overline{B}^0}(p_T)=\frac{\mathcal{B}(\Lambda_b^0\to J/\psi pK^-)}{\mathcal{B}(\overline{B}^0\to J/\psi\overline{K}^{*0})}f_{\Lambda_b^0}/f_d(p_T)\equiv\mathcal{S}\,f_{\Lambda_b^0}/f_d(p_T), \quad (8)$$

where $\mathcal{S}\equiv\mathcal{B}(\Lambda_b^0\to J/\psi pK^-)/\mathcal{B}(\overline{B}^0\to J/\psi\overline{K}^{*0})$ is a constant factor, which can be determined from the fit in Fig. 6. The absolute branching fraction of the decay $\Lambda_b^0\to J/\psi pK^-$ can then be measured as

$$\mathcal{B}(\Lambda_b^0\to J/\psi pK^-)=\mathcal{S}\,\mathcal{B}(\overline{B}^0\to J/\psi\overline{K}^{*0}). \quad (9)$$

The average of the fit results for the 7 and 8 TeV samples gives $\mathcal{S}=0.2458\pm0.0030$, which results in

$$\mathcal{B}(\Lambda_b^0\to J/\psi pK^-)=\left(3.17\pm0.04\pm0.07\pm0.34^{+0.45}_{-0.28}\right)\times10^{-4}.$$

The first uncertainty is statistical, the second is systematic, the third is due to the uncertainty on the branching fraction of the $\overline{B}^0\to J/\psi\overline{K}^{*0}$ decay, and the fourth is due to the knowledge of $f_{\Lambda_b^0}/f_d$.

In Ref. [11] the ratio $\mathcal{B}(\Lambda_b^0\to J/\psi p\pi^-)/\mathcal{B}(\Lambda_b^0\to J/\psi pK^-)$ was reported. Combining this with the value of $\mathcal{B}(\Lambda_b^0\to J/\psi pK^-)$ above, the branching fraction of $\Lambda_b^0\to J/\psi p\pi^-$ is determined as

$$\mathcal{B}(\Lambda_b^0\to J/\psi p\pi^-)=(2.61\pm0.09\pm0.13^{+0.47}_{-0.37})\times10^{-5},$$

where the first uncertainty is statistical, the second is due to the systematic uncertainty on $\mathcal{B}(\Lambda_b^0\to J/\psi p\pi^-)/\mathcal{B}(\Lambda_b^0\to J/\psi pK^-)$, and the third is due to systematic uncertainty on $\mathcal{B}(\Lambda_b^0\to J/\psi pK^-)$.

Two pentaquark-charmonium states, $P_c(4380)^+$ and $P_c(4450)^+$, were observed by LHCb in the amplitude analysis of the $\Lambda_b^0\to J/\psi pK^-$ decay [10], and the fractions $f(P_c^+)$ of the two pentaquark-charmonium states in the $\Lambda_b^0\to J/\psi pK^-$ decay were measured. Using these fractions and the value of $\mathcal{B}(\Lambda_b^0\to J/\psi pK^-)$ obtained in this analysis, the branching fractions $\mathcal{B}(\Lambda_b^0\to P_c^+K^-)\mathcal{B}(P_c^+\to J/\psi p)$ are calculated as

$$\mathcal{B}(\Lambda_b^0\to P_c^+K^-)\mathcal{B}(P_c^+\to J/\psi p)=f(P_c^+)\mathcal{B}(\Lambda_b^0\to J/\psi pK^-)=\begin{cases}(2.66\pm0.22\pm1.33^{+0.48}_{-0.38})\times10^{-5} & \text{for } P_c(4380)^+,\\ (1.30\pm0.16\pm0.35^{+0.23}_{-0.18})\times10^{-5} & \text{for } P_c(4450)^+,\end{cases}$$

where the first uncertainty is statistical, the second is due to the systematic uncertainty on $f(P_c^+)$, and the third is due to the systematic uncertainty on $\mathcal{B}(\Lambda_b^0\to J/\psi pK^-)$.

11 Conclusion

Using a data sample corresponding to an integrated luminosity of $3\,fb^{-1}$ collected by the LHCb detector in 2011 and 2012, the product of the Λ_b^0 differential production cross-section and the branching fraction of the decay $\Lambda_b^0\to J/\psi pK^-$ is measured as a function of the Λ_b^0 baryon's transverse momentum and rapidity. The product of the $\overline{B}^0$ differential production cross-section and the branching fraction of the decay $\overline{B}^0\to J/\psi\overline{K}^{*0}$ is also measured. The kinematic region of the measurements is $p_T<20$ GeV/c and $2.0<y<4.5$.

The ratios of the cross-sections at $\sqrt{s}=8$ TeV to those at $\sqrt{s}=7$ TeV are calculated for Λ_b^0 and $\overline{B}^0$ hadrons and are compared with FONLL predictions. The p_T dependence of the ratios is consistent with the FONLL calculations, while the y dependence is not consistent. The production ratios of the Λ_b^0 and $\overline{B}^0$ hadrons are given for the 2011 and 2012 samples separately, and are consistent with the dependence on p_T and y of the b hadron observed in a previous LHCb analysis. The asymmetry a_{p+d} between Λ_b^0 and $\overline{\Lambda}_b^0$ is also measured as a function of p_T and y. The result suggests some baryon number transport from the beam particles to the Λ_b^0 baryons.

Using information on the fragmentation ratio $f_{\Lambda_b^0}/f_d$ from a previous LHCb measurement, the absolute branching fraction $\mathcal{B}(\Lambda_b^0\to J/\psi pK^-)$ is obtained. Using previous LHCb measurements, the branching fractions $\mathcal{B}(\Lambda_b^0\to J/\psi p\pi^-)$ and $\mathcal{B}(\Lambda_b^0\to P_c^+K^-)\mathcal{B}(P_c^+\to J/\psi p)$ are determined.

We thank J. L. Rosner for interesting discussions of asymmetry in beauty baryon production. We express our gratitude to our colleagues in the CERN accelerator departments for the excellent performance of the LHC. We thank the technical and administrative staff at the LHCb institutes. We are indebted to the communities behind the multiple open source software packages on which we depend. We are also thankful for the computing resources and the access to software R&D tools provided by Yandex LLC (Russia).

Appendix

Table 3. Products of Λ_b^0 production cross-sections (pb) and the branching fraction $\mathcal{B}(\Lambda_b^0 \to J/\psi p K^-)$ in bins of p_T and y in the 2011 data sample. The first uncertainties are statistical and the second are systematic.

$p_T/(\mathrm{GeV}/c)$	$2.0<y<2.5$	$2.5<y<3.0$	$3.0<y<3.5$
0−3	326±42±44	354±18±23	319±14±20
3−4	439±58±54	503±27±33	486±22±31
4−5	445±48±48	425±21±27	376±17±22
5−6	411±39±45	297±15±17	296±13±17
6−7	224±23±24	235±12±14	203±10±12
7−8	162±17±16	175± 9±11	145±7.4±9.2
8−9	100±12± 9	109±6.5±7.0	92.7±5.5±6.3
9−10	83.2±9.7±8.1	93.6±6.0±6.4	63.6±4.4±4.6
10−12	53.6±4.6±4.3	39.5±2.3±2.4	29.0±1.8±1.9
12−20	11.4±0.8±0.7	11.3±0.6±0.6	8.6±0.6±0.6
	$3.5<y<4.0$	$4.0<y<4.5$	
0−3	244±13±19	221±26±35	
3−4	371±21±32	231±29±38	
4−5	294±16±22	138±18±19	
5−6	229±12±17	95±14±16	
6−7	151± 9±12	61±11± 8	
7−8	99.0±6.5±8.1	38.4±0.8±6.2	
8−9	69.0±5.3±5.9	37.7±7.7±5.9	
9−10	43.3±4.1±4.2	22.8±5.8±4.0	
10−12	20.4±1.9±1.7	7.8±1.8±1.2	
12−20	4.0±0.4±0.4	2.2±0.6±0.5	

Table 4. Products of Λ_b^0 production cross-sections (pb) and the branching fraction $\mathcal{B}(\Lambda_b^0 \to J/\psi p K^-)$ in bins of p_T and y in the 2012 data sample. The first uncertainties are statistical and the second are systematic.

$p_T/(\mathrm{GeV}/c)$	$2.0<y<2.5$	$2.5<y<3.0$	$3.0<y<3.5$
0−1	100±29±33	159±20±27	157±15±22
1−2	465±64±88	487±29±50	433±24±46
2−3	661±63±120	648±30±58	541±22±41
3−4	706±51±94	715±25±52	559±18±38
4−5	579±39±68	624±20±39	417±12±27
5−6	463±28±47	446±14±28	356±10±23
6−7	318±20±29	322±10±20	210± 7±12
7−8	248±15±23	236± 8±15	159± 5±10
8−9	173±11±18	140.7±5.4±9.2	118.4±4.4±7.8
9−10	130± 9±13	92.6±3.9±6.3	65.4±2.9±4.4
10−12	81.3±4.5±7.0	57.1±2.1±3.4	38.1±1.5±2.4
12−20	15.2±0.7±1.0	13.7±0.5±0.8	9.5±0.4±0.6
	$3.5<y<4.0$	$4.0<y<4.5$	
0−1	141±18±33	108±29±51	
1−2	269±20±41	222±36±52	
2−3	427±21±48	234±28±43	
3−4	393±17±34	256±25±45	
4−5	324±12±27	195±17±26	
5−6	229± 9±16	111±11±16	
6−7	152± 7±11	99±10±14	
7−8	114± 5± 9	51.3±5.8±6.4	
8−9	74.7±4.2±6.1	30.8±5.0±5.0	
9−10	55.4±3.5±5.4	17.4±3.5±2.9	
10−12	27.7±1.7±2.3	10.3±1.6±1.4	
12−20	6.1±0.4±0.5	1.4±0.4±0.2	

Table 5. Products of $\overline{\mathrm{B}}^0$ production cross-sections (pb) and $\mathcal{B}(\overline{\mathrm{B}}^0 \to \mathrm{J/\psi}\overline{\mathrm{K}}^{*0})$ in bins of p_{T} and y in the 2011 data sample. The first uncertainties are statistical and the second are systematic.

$p_{\mathrm{T}}/(\mathrm{GeV}/c)$	$2.0<y<2.5$	$2.5<y<3.0$	$3.0<y<3.5$
0−3	2850±130±200	2870±50±140	2580±30±110
3−4	4420±220±340	4350±80±220	3740±60±170
4−5	3540±160±250	3570±60±160	3310±50±150
5−6	2620±100±170	2920±50±130	2330±40±100
6−7	2290± 80±150	2150±40±100	1820±30± 80
7−8	1790± 70±110	1630±30± 80	1320±20± 60
8−9	1260± 50± 80	1150±20± 60	877±17± 42
9−10	853± 34± 53	862±19± 43	613±14± 31
10−12	581± 17± 32	540±10± 25	411± 8± 20
12−20	172± 4± 8	141± 2± 6	102± 2± 5
	$3.5<y<4.0$	$4.0<y<4.5$	
0−3	2110±30± 90	1450±40± 80	
3−4	2660±50±130	1790±70±130	
4−5	2310±40±110	1460±60±110	
5−6	1750±30± 80	1050±40± 80	
6−7	1190±30± 60	608±30± 48	
7−8	853±20± 45	573±29± 51	
8−9	650±18± 37	385±21± 38	
9−10	424±14± 27	207±15± 23	
10−12	258± 7± 15	96± 6± 9	
12−20	64± 2± 4	26± 2± 3	

Table 6. Products of $\overline{\mathrm{B}}^0$ production cross-sections (pb) and $\mathcal{B}(\overline{\mathrm{B}}^0 \to \mathrm{J/\psi}\overline{\mathrm{K}}^{*0})$ in bins of p_{T} and y in the 2012 data sample. The first uncertainties are statistical and the second are systematic.

$p_{\mathrm{T}}/(\mathrm{GeV}/c)$	$2.0<y<2.5$	$2.5<y<3.0$	$3.0<y<3.5$
0−1	1260±110±200	1240±40± 80	1100±30± 60
1−2	3340±170±340	3360±60±170	3200±50±150
2−3	5860±220±600	4930±70±240	4100±50±180
3−4	6650±200±550	5010±60±240	4150±50±180
4−5	4560±120±310	4340±50±190	3400±40±140
5−6	4260±100±280	3550±40±160	2730±30±120
6−7	2830± 60±170	2560±30±110	1960±20± 80
7−8	2270± 50±140	1810±20± 80	1460±20± 70
8−9	1650± 40±100	1460±20± 70	1100±10± 50
9−10	1180± 30± 70	1070±20± 50	696±10± 34
10−12	707± 13± 38	614± 7± 27	489± 6± 23
12−20	246± 3± 11	180± 2± 8	129± 2± 6
	$3.5<y<4.0$	$4.0<y<4.5$	
0−1	1010±30± 60	754±45± 73	
1−2	2830±50±150	1720±60±140	
2−3	3200±50±160	2460±80±200	
3−4	3180±40±150	1770±50±130	
4−5	2610±30±120	1650±50±120	
5−6	1900±30± 90	1280±40±100	
6−7	1500±20± 70	816±26± 60	
7−8	1030±20± 50	621±22± 52	
8−9	711±13± 38	390±15± 34	
9−10	478±10± 28	301±13± 31	
10−12	312± 6± 18	137± 5± 12	
12−20	82± 2± 5	36± 2± 3	

Table 7. Asymmetries $a_{\rm p+d}$ (%) of $\Lambda_{\rm b}^0$ and $\overline{\Lambda}_{\rm b}^0$ in bins of $p_{\rm T}$ and y for the 2011 and 2012 samples. The first uncertainties are statistical and the second are systematic.

	2011	2012
$p_{\rm T}/({\rm GeV}/c)$		
0−1	−5.9±9.4±7.0	−14.5±6.4±5.0
1−2	+2.7±4.9±4.4	−4.9±3.4±3.5
2−3	−0.1±3.6±3.3	−0.6±2.5±2.4
3−4	−4.5±2.9±2.6	−4.2±2.0±1.9
4−5	−1.3±2.7±2.2	−1.1±1.8±1.7
5−6	−1.3±2.7±2.3	−0.5±1.8±1.3
6−7	+2.7±2.9±1.9	−2.7±1.9±1.2
7−8	+5.3±3.1±1.7	−1.3±2.0±1.0
8−9	−4.4±3.5±1.9	−0.3±2.3±1.6
9−10	−5.8±4.0±1.2	+1.6±2.6±0.9
10−12	+1.1±3.6±2.1	+2.3±2.2±2.0
12−20	+2.7±3.4±0.8	+0.6±2.2±0.5
y		
$2.0<y<2.5$	−6.0±3.3±3.1	−7.6±2.0±1.2
$2.5<y<3.0$	−0.3±1.7±2.1	−0.3±1.1±0.9
$3.0<y<3.5$	−1.0±1.6±1.1	+0.7±1.1±1.0
$3.5<y<4.0$	+4.3±2.1±1.1	+2.4±1.5±1.2
$4.0<y<4.5$	+7.3±5.4±2.2	+8.4±3.7±1.9

References

1 S. H. Lee et al, Phys. Rev. Lett., **100**: 222301 (2008)
2 Y. Oh, C. M. Ko, S. H. Lee, and S. Yasui, Phys. Rev. C, **79**: 044905 (2009)
3 W. S. Lockman et al, Phys. Lett. B, **85**: 443 (1979)
4 P. Chauvat et al (R608 Collaboration), Phys. Lett. B, **199**: 304 (1987)
5 S. Chatrchyan et al (CMS Collaboration), Phys. Lett. B, **714**: 136 (2012)
6 J. L. Rosner, Phys. Rev. D, **90**: 014023 (2014)
7 R. Aaij et al (LHCb Collaboration), Phys. Rev. D, **85**: 032008 (2012)
8 R. Aaij et al (LHCb Collaboration), JHEP, **08**: 143 (2014)
9 R. Aaij et al (LHCb Collaboration), Phys. Rev. Lett., **111**: 102003 (2013)
10 R. Aaij et al (LHCb Collaboration), Phys. Rev. Lett., **115**: 072001 (2015)
11 R. Aaij et al (LHCb Collaboration), JHEP, **07**: 103 (2014)
12 K. Abe et al (Belle Collaboration), Phys. Lett. B, **538**: 11 (2002)
13 A. A. Alves Jr. et al (LHCb Collaboration), JINST, **3**: S08005 (2008)
14 R. Aaij et al (LHCb Collaboration), Int. J. Mod. Phys. A, **30**: 1530022 (2015)
15 R. Aaij et al, JINST, **9**: P09007 (2014)
16 R. Arink et al, JINST, **9**: P01002 (2014)
17 M. Adinolfi et al, Eur. Phys. J. C, **73**: 2431 (2013)
18 A. A. Alves Jr. et al, JINST, **8**: P02022 (2013)
19 R. Aaij et al, JINST, **8**: P04022 (2013)
20 K. A. Olive et al (Particle Data Group), Chin. Phys. C, **38**: 090001 (2014)
21 T. Sjöstrand, S. Mrenna, and P. Skands, JHEP, **05**: 026 (2006)
22 T. Sjöstrand, S. Mrenna, and P. Skands, Comput. Phys. Commun., **178**: 852 (2008)
23 I. Belyaev et al, J. Phys. Conf. Ser., **331**: 032047 (2011)
24 D. J. Lange, Nucl. Instrum. Methods A, **462**: 152 (2001)
25 P. Golonka and Z. Was, Eur. Phys. J. C, **45**: 97 (2006)
26 J. Allison et al (Geant4 Collaboration), IEEE Trans. Nucl. Sci., **53**: 270 (2006)
27 S. Agostinelli et al (Geant4 Collaboration), Nucl. Instrum. Methods A, **506**: 250 (2003)
28 M. Clemencic et al, J. Phys. Conf. Ser., **331**: 032023 (2011)
29 L. Breiman, J. H. Friedman, R. A. Olshen, and C. J. Stone, *Classification and regression trees* (Belmont, California, USA: Wadsworth international group, 1984)
30 B. P. Roe et al, Nucl. Instrum. Methods A, **543**: 577 (2005)
31 R. E. Schapire and Y. Freund, Jour. Comp. and Syst. Sc., **55**: 119 (1997)
32 A. Hoecker et al, PoS, **ACAT**: 040 (2007)
33 R. Fruhwirth, Nucl. Instrum. Methods A, **262**: 444 (1987)
34 M. Needham and J. Van Tilburg, LHCb -2007-020
35 M. Needham, LHCb -2007-129
36 R. Aaij et al (LHCb Collaboration), JINST, **9**: P12005 (2014)
37 W. D. Hulsbergen, Nucl. Instrum. Methods A, **552**: 566 (2005)
38 R. Aaij et al (LHCb Collaboration), JHEP, **08**: 117 (2013)
39 R. Aaij et al (LHCb Collaboration), Phys. Rev. D, **88**: 052002 (2013)
40 M. Pivk and F. R. Le Diberder, Nucl. Instrum. Methods A, **555**: 356 (2005)
41 R. Aaij et al (LHCb Collaboration), JHEP, **07**: 041 (2014)
42 D. Martínez Santos and F. Dupertuis, Nucl. Instrum. Methods A, **764**: 150 (2014)
43 R. Aaij et al (LHCb Collaboration), JINST, **10**: P02007 (2015)
44 C. Tsallis, J. Statist. Phys., **52**: 479 (1988)
45 C. Tsallis, Braz. J. Phys., **29**: 1 (1999)
46 A. A. Bylinkin and O. I. Piskounova, arXiv:1501.07706
47 G. D. Lafferty and T. R. Wyatt, Nucl. Instrum. Methods A, **355**: 541 (1995)
48 M. Cacciari, M. Greco, and P. Nason, JHEP, **05**: 007 (1998)
49 M. Cacciari, S. Frixione, and P. Nason, JHEP, **03**: 006 (2001)
50 M. Cacciari et al, JHEP, **10**: 137 (2012)
51 J. L. Rosner, Phys. Rev. D, **86**: 014011 (2012)